BIOCHEMISTRY
including biophysical chemistry & molecular biology

Article

pubs.acs.org/biochemistry

Enhanced Sampling Molecular Dynamics Identifies PrP^{Sc} Structures Harboring a C-Terminal β-Core

Pascal Baillod, Julian Garrec, Maria-Carola Colombo, Ivano Tavernelli, and Ursula Rothlisberger*

Laboratory of Computational Chemistry and Biochemistry, Ecole Polytechnique Fédérale de Lausanne, Lausanne, Switzerland

Supporting Information

ABSTRACT: We perform a replica exchange molecular dynamics simulation corresponding to a 2.8 μs total time for the extensive enhanced sampling of the conformational space of the C-terminal part (residues 124−226) of the mouse prion protein (PrP); 1.3% of the conformations sampled display a high level of β-structure ($\geq$19 residues), allowing the assessment of β-propensities along the sequence and highlighting the most structurally labile hot spots. A clustering algorithm is applied to sort the structures of this pool according to their fold. Ten β-rich folds are thus defined and analyzed with regard to their topology, accumulation temperatures, and structural characteristics. In contrast to the so-called spiral and β-helix models suggesting that the β-rich core of the scrapie isoform (PrP^{Sc}) comprises the N-terminal tail and part of the C-terminal domain up to helix 1 (H1), we present putative structural models for monomeric precursors of PrP^{Sc} and PrP β-oligomers that are characterized by a C-terminal β-rich core, in agreement with the suggestions of a series of recent experiments.

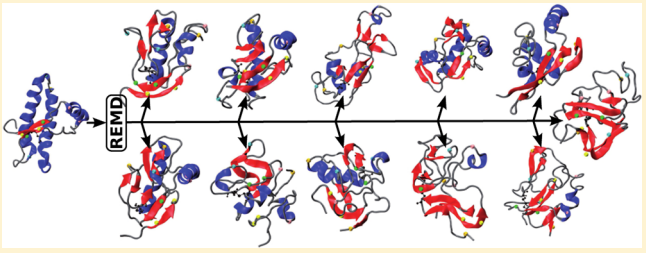

According to the prion hypothesis,[1,2] prion diseases are caused by an aggregated misfold of the prion protein (PrP) frequently termed scrapie isoform PrP^{Sc}. One proposed scenario for this transition assumes the normal cellular isoform (PrP^{C}) in equilibrium with a metastable intermediate, designated PrP*, that catalyzes the conversion.[3,4] This process is devoid of any chemical change but involves profound conformational alterations from the soluble, predominantly α-helical PrP^{C} to the insoluble, aggregated β-rich PrP^{Sc}.[5]

The first experimental PrP^{C} structure was obtained by nuclear magnetic resonance (NMR) for mouse PrP (residues 124−226)[6] (Figure 1, panel 0). The protein shows an unstructured N-terminal domain (residues 21−123) and a structured C-terminal domain (residues 124−226). PrP C-terminal domains of different species reveal highly conserved structures, comprised of two short β-strands (S1 and S2), three α-helices (H1−H3), a disulfide bridge connecting H2 and H3, and two glycosylation sites (one in H2 and one in the H2−H3 loop).

Despite decades of research, the structure of PrP^{Sc} has remained elusive.[7] Circular dichroism (CD) of the full length protein has revealed that PrP^{C} (6% β and 43% α) undergoes dramatic secondary structure changes in the conversion to PrP^{Sc} (43% β and 30% α).[5] For PrP27−30, a subfragment of PrP^{Sc} obtained with proteinase K digestion via cleavage around residues 87−91 (depending on the PrP strain), the corresponding values are 47−54% β and 17−25% α, respectively.[5,8,9] Consequently, PrP27−30 should contain at least ~17 α-helical residues.

A consensus is slowly emerging for the picture of a very complex PrP folding landscape, allowing for a large variety of misfolding pathways.[4,10−22] The multitude of possible conformations observed in vitro, under different perturbing environments (acidic pH,[23,24] redox condition changes,[10,25] chemical unfolding agents,[11−13,20] removal of detergent from the protein solution,[14,15,21] high temperature,[16] and pressure[4]) include a variety of soluble monomeric and oligomeric species,[17−19] as well as aggregated conformations and amyloid fibrils.[20,21]

The relationship between the size of PrP^{Sc} aggregates and infectivity has also been evaluated. Silveira and colleagues showed that small oligomers composed of fewer than six units were noninfectious in Syrian hamsters, while particles exhibiting the highest infectivity were nonfibrillar structures composed of 14−28 units of PrP^{Sc}.[26] β-Monomers,[19,25] predominantly α-monomers and α-dimers,[18,27] octamers,[17] 12mers and 36mers,[28] and 15mers[29] have also been observed in in vitro oligomerization experiments. Even though oligomerization may play a crucial role in the infective process, it is still unclear if the structural transition is induced by aggregation or if the structure of PrP by itself is intrinsically metastable under particular environmental conditions. This has triggered the quest for a monomeric PrP^{Sc} or PrP* precursor form,[4] as well as the investigation of PrP^{C} changes leading to such a form.[16]

Furthermore, several independent experiments have shown that the C-terminal structured domain might by itself be able to promote the pathology. (i) PrP27−30 is still infectious.[30] (ii) The structured C-terminal domain (residues 124−226) can also undergo complex misfolding conversions leading to β-

Received: August 13, 2012
Revised: November 9, 2012
Published: November 20, 2012

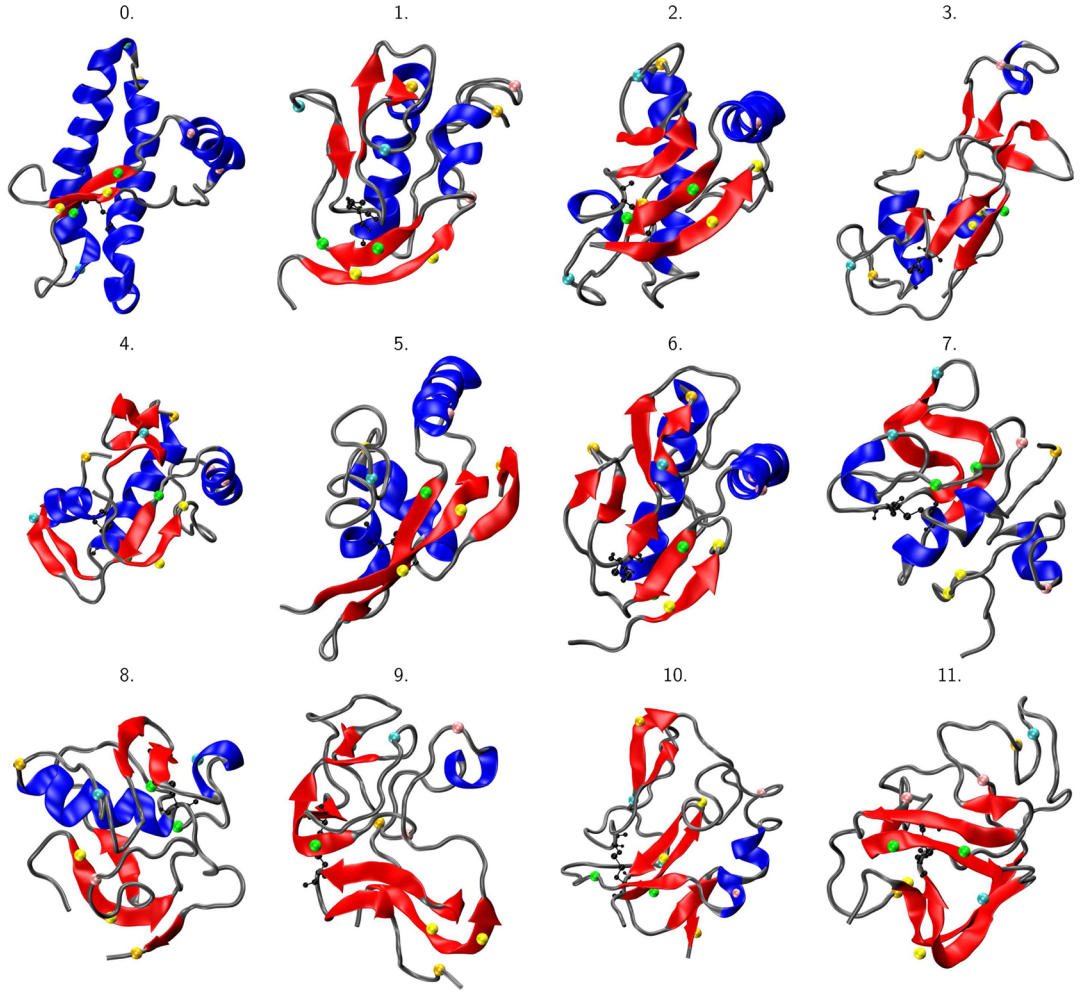

Figure 1. β-Rich folds. Panels 1−10 show representative structures of β-rich folds 1−10 as specified in Table 1. Panel 0 shows the NMR structure, and panel 11 shows the maximal β-content structure obtained in simulation (38 β-residues). Helices are colored blue and β-sheets red. To highlight the sequence positions of structural rearrangements, sequence portions spanning NMR secondary structure elements are highlighted with CPK sphere representations of the C-α atoms of the residues delimiting S1 (yellow), S2 (green), H1 (pink), H2 (cyan), and H3 (orange). The figures were all oriented in the same way as the NMR structure of panel 11.

sheet-rich oligomers and aggregates.[24,31,32] (iii) Limited proteolysis of fibrils formed in vitro with recombinant mouse PrP has generated C-terminal prion fragments that have been reported to support fibril propagation in vitro.[33] This unusual protease-resistant core reaches from residues 152−162 (C-terminus of H1 or S2) to residue 226 and has also been found in a novel form of sporadic Creutzfeldt-Jakob disease (CJD).[34] (iv) Lu et al., who performed hydrogen exchange and mass spectroscopy experiments on recombinant human PrP amyloid fibrils, identified a β-rich core comprising mainly H2 and H3 residues.[35] (v) Similar β-rich cores were found with recombinant human PrP fibrils formed in vitro and investigated via site-directed spin labeling experiments combined with EPR spectroscopy.[36] (vi) Fibril unfolding studies performed with labeled residues revealed two distinct cooperative unfolding domains differing with respect to their resistance to denaturation, with the more resistant domain coinciding with the β-rich core described above.[37] (vii) The binding of PrP and PrP^{Sc} specific antibodies to fibrils suggests that residues from the C-terminal domain are buried in the fibril structure, while residues from the N-terminal domain are solvent-exposed.[38]

Various atomistic fibril models of monomeric misfolded PrP or PrP^{Sc} have been proposed.[7] In the so-called spiral[39] and β-helix[40,41] models, the β-rich region comprises the N-terminal tail (spiral model) and part of the C-terminal domain up to H1 (β-helix model). Although these models are in good agreement with a number of experimental data, they have been subject to criticism because several lines of evidence now highlight the H2−H3 region as a possible β-core.[33,35−38] Rezaei and co-workers have isolated the H2−H3 domain as an independent folding unit and shown that this domain is highly fibrillogenic[24,42] and may act as a conformational switch in the full protein.[43] It has also been suggested that PrP^{Sc} could be entirely refolded in an in-register extended β-sheet.[44]

Using high-temperature molecular dynamics (MD) simulations, a number of transient β-enriched conformations have been observed.[45,46] A replica-exchange molecular dynamics (REMD) study has investigated early changes in the solvation shell and subdomain motions of murine PrP,[47] but no substantial β-structure enrichment was observed within the limited simulation time (30 ns) and temperature range (320−370 K).

In this work, we perform an extensive (2.8 μs total time) explicit solvent REMD[48] simulation to characterize the conformational landscape of the C-terminal part of monomeric PrP^{C} (residues 124−226). To allow for an efficient simulation

dx.doi.org/10.1021/bi301091x | *Biochemistry* 2012, 51, 9891−9899

despite the explicit solvent system investigated, we use an approximate REMD protocol (see Computational Methods). Our aim is to assess sequence specific β-sheet formation propensities of the monomeric PrP and to investigate possible β-rich rearrangements. To increase the probability of observing PrP^{Sc}-related changes, we have chosen to perform the simulations at pH 4, mimicking an acid environment favoring the PrP^{C} to PrP^{Sc} conversion;[23,49−52] 1.3% of all sampled configurations display a high β-content (>19 residues). These observed β-rich conformations can serve as structural models for putative monomeric precursors of PrP^{Sc} and/or β-oligomers, allowing the characterization of early stages of the pathology that, because of insolubility and aggregation, remain poorly understood.

COMPUTATIONAL METHODS

Molecular Dynamics Setup. The starting configuration was the mouse PrP NMR structure [residues 124−226, Protein Data Bank (PDB) entry 1AG2[6]]. The protonation states of ionizable side chains were predicted by finite-difference Poisson−Boltzmann calculations[53,54] to mimic a pH 4 environment, which is known to favor PrP misfolding.[49]

The solvent and protein dielectric constants were taken to be 80 and 8, respectively. DELPHI[55] supplied with the WHATIF package[56] was used to solve the Poisson−Boltzmann equation. The protonation states of His, Asp, and Glu side chains were consequently set as follows: His140, p; Asp144, d; Glu146, d; Asp147, d; Glu152, p; Asp167, p; His177, p; Asp178, d; His187, p; Glu196, d; Glu200, p; Asp202, d; Glu207, p; Glu211, p; Glu221, p (where p stands for protonated and d for deprotonated). A rhombic dodecahedron box with 14076 water molecules was constructed around the protein, and eight Cl^- ions were added to neutralize the system.

All simulations were performed with GROMACS-3.3.0,[57] the GROMOS96 43a1 force field,[58] the SPC explicit solvent water model,[59] and a MD time step of 1.5 fs. The length of covalent bonds involving hydrogen atoms was constrained by the SHAKE[60] algorithm with a tolerance of 10^{-4} kJ mol^{-1} nm^{-1}. Coulombic interactions were treated using a twin range cutoff, in which interactions within 1.0 nm, and between 1.0 and 1.4 nm were computed every MD step, and every five MD steps, respectively. Electrostatic interactions beyond 1.4 nm were approximated with a generalized reaction field[61] generated by a dielectric continuum with a dielectric constant of 66. van der Waals interactions were computed every step within a cutoff of 1.0 nm.

The equilibration of the system was performed in the *NPT* ensemble, using a Berendsen barostat with a time coupling constant of 1 ps.[62] The solvent was first equilibrated for 225 ps at 300 K with protein-atom position restraints of 25×10^3 kJ mol^{-1} nm^{-2}. Then, the protein was gradually heated to 300 K with six successive 50 ps MD runs, for which the increasing temperatures were 50, 100, 150, 200, 250, and 300 K and the decreasing protein atom position restraints were 25×10^3, 5×10^3, 3.75×10^3, 2.5×10^3, and 1×10^3 kJ mol^{-1} nm^{-2}. In the final stage, 3 ns of 300 K MD with no position restraints supplied the starting configuration for subsequent production runs.

Reference Molecular Dynamics Simulation. A reference MD simulation was run for 315 ns in the *NVT* ensemble using two Nosé-Hoover thermostats (one for the protein and one for solvent and counterions, with time coupling constants of 0.4 and 1.6 ps, respectively).[63,64] The main purpose of this simulation was (i) to establish a comparison, in terms of configurational sampling, between REMD and straightforward MD simulations and (ii) to check the validity of our approximate REMD protocol (see the next section).

REMD Simulations. To extend the conformational sampling, we used an approximate REMD method. REMD simulations of molecular systems solvated in explicit water require a large number of replicas to span a temperature interval sufficient for an efficient sampling of configuration space. This is mainly due to the very narrow energy distributions of the different replicas due to the large number of degrees of freedom associated with the solvent molecules. Therefore, a straightforward application of a REMD protocol will predominantly sample solvent degrees of freedom, which contribute with more than 99% to the total energy of the system. Several modified REMD protocols have been suggested for overcoming this problem. One of the most commonly used approaches is the so-called "hybrid-Hamiltonian" scheme.[65,66] In this approach, the full Hamiltonian (with explicit solvent) is used to propagate the equations of motion, while a simplified one, which neglects solvent−solvent interactions (as in the case of implicit solvent MD[67]), is used to compute the Monte Carlo (MC) switching probabilities between the different replicas at different temperatures. Previous studies[65,68,69] have shown that the bias induced in the final sampling by this approach is negligible. Here we follow this philosophy by using the protein potential energy (including its interaction energy with the solvent) as a simplified potential to compute the switching probabilities. A test of the validity of our approximate REMD protocol is given in the Supporting Information. It shows that the sampling is performed according to the proper Boltzmann distribution.

The REMD routine of GROMACS was modified to compute exchange probabilities with this simplified Hamiltonian, while the MD propagation is based on the usual total potential energy. Trial REMD simulations were performed with different temperature distributions for the replicas, to ensure similar exchange probabilities at all temperatures. The following temperature distribution was selected for the 32 replicas and used for the production run: 300.0, 306.0, 312.1, 318.2, 324.3, 330.4, 336.6, 342.8, 349.1, 355.3, 361.6, 368.0, 374.3, 380.7, 387.1, 393.6, 400.1, 406.6, 413.1, 419.7, 426.3, 432.9, 439.6, 446.3, 453.0, 459.8, 466.5, 473.3, 480.2, 487.1, 494.0, and 500.9 K. The REMD production run was conducted in the *NVT* ensemble for 88.4 ns (total aggregate time of 2.8 μs), with exchanges attempted every 60 ps, performed on adjacent temperature replicas n and $n + 1$ at every odd exchange trial, and $2n$ and $2n + 1$ at every even exchange trial.

The equilibration of the REMD replicas consisted of 32 parallel MD runs, linearly heating 32 copies of the initial configuration described above to the different temperatures in 300 ps. MD was continued for an additional 200 ps at these temperatures, generating the REMD starting replicas. Each of these 32 replicas was prolonged for 88.4 ns for data collection, leading to a total simulation time of 2.8 μs. This simulation length was based on the fact that after this time we do not seem to sample a significant amount of new conformational clusters. This is illustrated in one particular case by the evolution of the fraction of collapsed structures (radius of gyration of $\leq$1.3 nm) along our REMD simulations (Figure S4 and the text of the Supporting Information).

Secondary Structure Analysis and Clustering. The secondary structure content was calculated for each config-

dx.doi.org/10.1021/bi301091x | *Biochemistry* 2012, 51, 9891−9899

uration generated by our REMD simulations, using the DSSP[70] algorithm. To cluster the different β-rich folds (i.e., those containing $\geq$19 β-residues) as a function of the topology and location of the new β-sheets and to distinguish β-strands from β-sheets, we developed and applied the β-contact map clustering (*bcmc*) protocol. *bcmc* comprises the following three steps. (I) For each β-rich structure, a β-contact map (termed *bcm*) was computed with all β-residues. Each β-rich structure was thus represented by a 103 × 103 *bcm* matrix (where 103 is the sequence length of the PrP structure) containing, in entry (i,j), the minimal inter-residue backbone H-bond distance whenever i and j were β-residues and "0" if either i or j were not a β-residue. Minimal inter-β-residue distances were only retained as β-contacts if (i) β-residues i and j were at least two residues apart in sequence, defining a possible contact between two distinct β-strands, and (ii) their distance was $\leq$0.35 nm. For nonretained distances, the corresponding position of the *bcm* matrix was set to "0". The *bcm* obtained with this procedure describes pairs of β-strands forming sheets (native and novel) found in the β-rich structures.

Then, (II) to simplify our analysis, we grouped the β-contacts by subdividing the sequence into intervals approaching an optimal target size of I_r residues. The number of intervals (s) was obtained by rounding $103/I_r$ to the next integer. Every residue i was assigned to an interval of which the identifier number I_i was obtained by rounding $(i/103) \times s$ to the next integer. At this stage, each β-rich structure was represented by an $s \times s$ simplified *bcm* matrix (*sbcm*). Each *sbcm* was constructed by setting $sbcm(I_i,I_j)$ to "1" whenever any pair of residue $i \in$ interval I_i and $j \in$ interval I_j would form a β-contact $[bcm(i,j) = 1]$ and to zero if no such pair could be found. Alternatively, an *sbcm* matrix element of "1" means that two distinct segments of the sequence contain H-bonded β-residues. The *sbcm* is the fingerprint of the β-strand arrangement in a given β-rich structure.

Finally, (III) to cluster our REMD structures according to their β-sheet pattern, we clustered the *sbcm*s using K-means nonhierarchical clustering,[71] as implemented in MATLAB.[72]

A number of trials were performed, varying the target number of clusters, I_r, and the size of the simplified matrix to obtain the smallest possible number of clusters containing the same *sbcm* for all members. This led to an I_r of 15, an s of 7, and a target number of clusters of 4500, of which a majority were small. Clusters were assigned to group α+ whenever they contained at least one structure with 17 α-helical residues (the minimal α-helical content of PrP^{Sc}) and to group $\alpha-$ otherwise. To limit the analysis to frequent β-sheet pairing patterns and stable folds, cluster population size threshholds were set as low as 20 for α+ clusters (so that very rare but potentially PrP^{Sc}-related folds could be considered) and to 182 for $\alpha-$ clusters. Finally, similar clusters (similar *bcm* and three-dimensional structures) with populations exceeding size threshholds were grouped into eight α+ (at least one α+ cluster) and two $\alpha-$ (no α+ cluster) folds. Thus, each fold contained clusters sharing a common group of β-contacts, with each cluster showing an additional alternative β-contact.

RESULTS AND DISCUSSION

Conformational Landscape. In our REMD simulations, statistics were collected from 32 trajectories of 88.4 ns each, distributed over a temperature range of 300−500 K. Figure 2 compares the conformational landscapes covered by three of these replicas (300, 361, and 500 K) and the first 88.4 ns of our reference MD simulation (i.e., without enhanced sampling). The conformational landscape is computed as a projection on the fraction of native contacts and the radius of gyration. As can be seen from the top panels of Figure 2, our REMD protocol allows an extended sampling with respect to a straightforward MD simulation of the same length and at the same temperature. A complete sampling of the phase space, which would include the unfolded state of the protein (small fraction of native contacts and high radius of gyration), is not possible because it would require much longer simulations. Nevertheless, our REMD simulations were long enough to capture many misfolded states, as we shall see in the remainder of this paper.

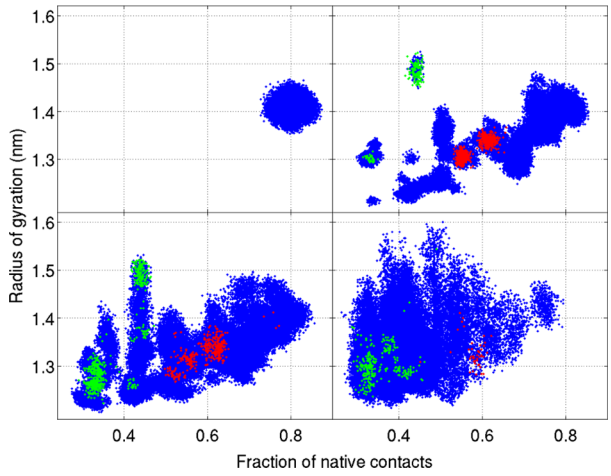

Figure 2. Conformational landscape computed as a projection on the fraction of native contacts and the radius of gyration. Two residues were considered to be in contact if the shortest distance between two atoms of these residues was <0.45 nm, and the fraction of native contacts of a given conformation was defined as the percentage of contacts of the NMR structure that were still present. α+ (red dots) and $\alpha-$ (green dots) are β-rich structures ($\geq$19 β-residues) with respective numbers of α-helix residues of $\geq$17 and <17: top left, reference MD at 300 K (88.4 ns trajectory, as REMD); top right, REMD at 300 K; bottom left, REMD at 361 K; bottom right, REMD at 500 K.

Part of the conformational landscape observed in REMD simulations is characterized by the occurrence of collapsed structures, which is in agreement with the results of Kuwata et al., that show that high-pressure unfolding is concomitant with protein collapse around molecular voids the authors identify within H2 and H3.[4] Because simulations are performed in the *NVT* ensemble, higher pressures build up at elevated temperatures (up to 3.6 kbar at 500 K, comparable with the high-pressure unfolding described above). The new structures obtained from our REMD simulations correspond to a strong misfolding of the native state, as we shall see in the next sections.

Secondary Structure Propensity. To assess the secondary structure propensity along the sequence, we computed the fraction of simulation time spent per residue in α- and β-conformations (Figure 3). H1 is found to be the most stable helix, followed by H3 and H2 whose C-terminal parts unravel (Figure 3, top panel), consistent with experimental stability studies[4,35,73,74] and results from other simulations.[47,75] This suggests that H1 might remain intact in PrP^{Sc} and constitute part of the minimal observed α-helical content of 17 residues.

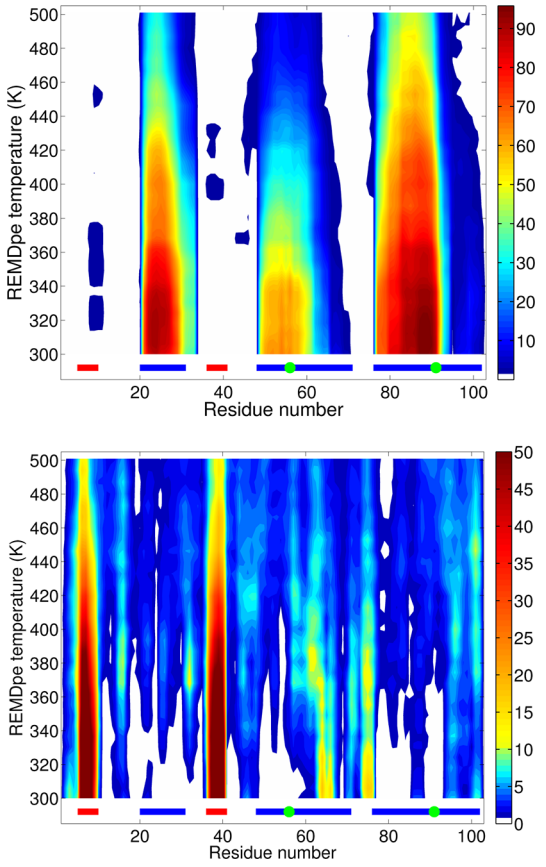

Figure 3. Secondary structure propensity per residue computed as a fraction of time (% indicated by the color bar) that each residue spends in a α-conformation (top panel) or a β-conformation (bottom panel) at all REMD temperatures. The colored rulers just below the x-axis show NMR α-helices (blue) and β-sheets (red), with green circles indicating the location of the disulfide bridge-forming Cys residues. Residues were numbered starting from the first residue of the NMR PDB file.

This is also supported by the decrease in α-helical content and unchanged β-content observed upon proteinase K digestion of recombinant PrP27−30 amyloid, leading to a smaller protease-resistant core and cleaving and/or degrading residues N-terminal to the C-terminus of H1.[33]

Remarkably, besides the mere loss of native structure at elevated temperatures, new β-sheets form occasionally, in particular in the C-terminal part of H2 and in the loop connecting H2 to H3 (Figure 3, bottom panel). In fact, 38.3, 6.75, and 1.29% of all structures (at all temperatures) have a β-content exceeding 7, 13, and 18 residues, respectively. Surprisingly, every residue of the sequence adopts a β-conformation at least once during the simulation (Figure 3, bottom panel), generating a variety of β-rich folds and revealing the intrinsic propensity of PrP124−226 to adopt β-rich conformations even in its monomeric form. Furthermore, the new β-sheets are essentially formed by residues belonging to H2 and H3 in the native structure (Figure 2, bottom panel), in agreement with the suggestion from independent experiments that the β-rich core of fibril β-sheets is located in the H2−H3 sequence interval.[24,33,35−38,43] In particular, our data are consistent with the finding of Rezaei and co-workers, according to which the H2−H3 domain is highly fibrillogenic[24,42] and may act as a conformational switch in the full protein.[43]

β-Rich Folds. We collected all structures with a β-content exceeding 18 residues (~1.3% of the total of sampled configurations) into a β-rich pool. To identify the major β-rich folds, we developed and applied the β-contact map clustering (*bcmc*) protocol, presented in detail in Computational Methods. Briefly, for each β-rich structure, a β-contact map (*bcm*) derived from a two-dimensional residue−residue distance plot was computed to describe pairs of hydrogen-bonded β-residues (identified by their sequence position) forming double- or multiple-stranded β-sheets. The *bcm* matrices were then clustered and classified into α+ (≥17 α-helical residues, which correspond to the experimentally observed α-helical content of PrP^{Sc}) and α− (otherwise) groups. The 10 major folds defined with this procedure contained 56.7% of the β-rich pool (Table 1) and 74.9 and

Table 1. Folds Obtained via *bcmc* Clustering of the β-Rich Pool (~1.3% structures with ≥19 β-residues)[a]

	F	%	max β	SASA increase
α+	1	17	31	23
	2	0.93	21	14
	3	8.9	25	14
	4	16.58	30	29
	5	0.77	28	17
	6	0.08	22	−3
	7	0.45	21	69
	8	0.11	25	21
α−	9	9.9	36	29
	10	2.19	26	40

[a]The α+ group includes folds containing at least one α+ structure with ≥17 α-helical residues. The α− group includes folds that only contain structures with fewer α-helical residues. F is the fold number. A minimal size of 182 members defines clusters forming the main folds (all except 6−8), while a smaller threshhold of 20 members is used to identify small α+ clusters (containing at least one α+ structure), grouped into additional folds 6−8. % is the fraction of the structures of the β-rich pool per fold. max β is the maximal number of β-residues observed in a structure of the fold. SASA increase is the increase in hydrophobic SASA (in %) with respect to the native fold.

51.1% of all α+ and α− structures, respectively. In Figure 1, one representative conformation is shown for each fold. The *bcm*'s of all folds are given in the Supporting Information and describe, for every β-strand, sequence location and the hydrogen-bonding partner β-strands. The atomic coordinates of these models (PDB format) are available in the Supporting Information.

All β-rich structures form at high temperatures, but fold 2 and fold 4 are the only ones to accumulate at room temperature; all other folds remain marginally stable at intermediate or high temperatures only. Fold 2 is characterized by the native β-sheet and two new β-strands: S3, formed at mid-H2, and S4, formed at the C-terminus of H2, forming the four-stranded β-sheet (S1−S2−S3−S4). Fold 4 is characterized by three distinct, noninteracting β-sheets: (i) the native S1−S2, (ii) S3, at the S2−H2 loop, hydrogen-bonded to S6, at the C-terminus of the protein, and (iii) S4, at the C-terminus of H2, hydrogen-bonded to S5, at the H2−H3 loop.

Transient β-sheet formations leading to structures similar to fold 4 were also observed when we prolonged our reference MD simulation from 88.4 ns (the simulation time of our REMD replica) to ~300 ns (Figure S2 of the Supporting Information). This conformational transition is most probably

dx.doi.org/10.1021/bi301091x | *Biochemistry* 2012, 51, 9891−9899

favored by (i) the low pH that is known to accelerate PrP misfolding[23,49−52] and (ii) the GROMOS force field that has a tendency to favor β-sheets with respect to α-helices.[76] We stress that we made this choice for the computational setup on purpose, to accelerate the transition toward β-rich folds. Although this can shift artificially the thermodynamic balance between different protein folds (hence, the relative probability densities in Figure 2 should be considered with caution), we consider it as a useful "trick" in helping to reveal β-rich folds on the conformational landscape of PrP.

The transition toward fold 4 observed in the reference MD simulation is completed only after ∼200 ns (Figure S2 of the Supporting Information), which is more than twice the simulation time of our REMD replica. This, once again, reflects the higher efficiency of our REMD protocol in terms of sampling efficiency. Nonetheless, the fact that fold 4 can be reached in a straightforward MD simulation is an indication of the ease by which PrP can reach it with respect to other β-rich folds.

Furthermore, fold 4 is one of the most frequent β-rich folds in our REMD simulations [∼17%, comparable in abundance only to fold 1 (Table 1)]. In contrast, folds 1, 3, and 5−10 possibly never exist at room temperature or require aggregation to larger multimers to be stabilized. Folds 2 and 4 could therefore be monomeric precursors on the pathway to a stable and soluble prion conformation, a β-oligomeric form that has been reported to form on the time scale of hours to days in stock solutions without prior denaturing treatment.[12] It has even been suggested that this form is in fact the global free energy minimum in aqueous solution.[14,15,17]

We have also characterized the different folds according to their location on the conformational landscape computed as a projection on the fraction of native contacts (Q_{fr}) and the radius of gyration (R_g) (Figure 2). It turns out that fold 3 is an elongated conformation, containing structures with R_g values as high as 1.6 nm (Figure 3, green and very rare red dots at R_g ∼ 1.5 nm), while the R_g values of all other folds range from ∼1.4 nm (such as fold 4, with an R_g that is close to that of the native fold) to 1.25 nm (highly collapsed structures, such as folds 1 and 10). Only folds 2, 4, and 5 contain structures with a Q_{fr} as high as 60−80%. While folds 2 and 4 accumulate at lower temperatures, fold 5 accumulates around 343 K. In other words, the only β-rich folds that can accumulate at low temperatures are nativelike folds. The native structure group has indeed the lowest average potential energy (total and protein), compared to the corresponding values for other structural groups, such as collapsed, unfolded, etc. (data not shown).

The monomeric β-rich core of a *bcmc* fold can be considered as the sum of all the residues that can adopt a β-conformation in at least one of the structures assigned to that fold. β-Rich cores were computed according to this assumption for all 10 *bcmc* folds (data not shown). With the exception of fold 5, the largest part of all β-cores coincides with the recently determined location of the β-core in fibrils, involving H2 and H3.[24,33,35−38,43] The α+ folds (1−4 and 6−8) can therefore be regarded as models of monomeric PrP^{Sc}.

The highest β-content we observe in our simulation comprises 38 residues for a rare α− structure that was not assigned to a fold (Figure 1, panel 12) and 31 residues for an α+ fold (fold 1, Table 1). Most of the β-content observed in our simulation originates from residues of the experimental β-rich cores observed in fibrils,[33,35−38] and further extension of the β-sheets we observe might occur via aggregation. This result is comparable to the maximal β-content of 38 residues achieved in the MD simulations that lead to the spiral model.[39,77,78] However, the β-rich core of the latter is located in the N-terminal part of the protein, in contradiction to the experimentally found C-terminal β-rich cores. The spiral model might nevertheless be a part of the conformational landscape of the monomer. With fold 5, we observe some of its features (all helices partially preserved, an extended native β-sheet, and a new β-strand located in the S2−H1 loop), but this *bcmc* fold is one of the rarest we obtain and is present only at high temperatures.

Finally, it is interesting to notice that all the β-rich structures we have obtained (Figure 1) exhibit some signatures of aggregation-prone macromolecules. (i) They all exhibit at least one exposed β-sheet edge that, according to Richardson et al.,[79] makes them more prone to binding other monomers (or a growing fibril) via backbone H-bonds. (ii) Except for fold 6, they are characterized by an increase in hydrophobic SASA ranging from ∼14 to ∼69% (Table 1). These criteria could be used in subsequent studies to build models of PrP^{Sc} oligomers or fibrils. The coordinates of the representative structures depicted in Figure 1 are given in the Supporting Information.

CONCLUSION

Using REMD simulations, we have performed an extensive exploration of the conformational landscape of the monomeric PrP C-terminal domain. A small fraction of all conformations sampled (1.3%) contain a high number (≥19) of β-residues. Clustering these structures according to their β-sheet arrangement has revealed 10 different β-rich folds, but only two of them accumulate at room temperature. Interestingly, most of these β-rich folds, including those that are present at room temperature, are in good agreement with the α- and β-content estimated from previous CD experiments.[5,8,9] They exhibit exposed β-sheet edges[79] and increased hydrophobic SASA, which is characteristic of proteins prone to aggregation. Therefore, our study provides putative structural models for the β-rich metastable intermediate (PrP*) that has been proposed as a possible catalyst for the $PrP^{C} \rightarrow PrP^{Sc}$ conversion.[3,4]

Although rare, β-rich conformations could be sampled in sufficient amounts to estimate β-propensities along the sequence. These calculations reproduce the general trend observed in a series of independent experiments, suggesting that the β-rich core of PrP^{Sc} corresponds to the H2−H3 sequence in native PrP^{C}.[24,33,35−38,42,43] This finding is in disagreement with the spiral[39] and β-helix[40,41] fibril models, which have been subject to controversy (see, e.g., ref 44).

One possible source of errors in this study is the GROMOS force field because it may favor β-sheets with respect to α-helices.[76] Nevertheless, the agreement with a broad range of experimental data suggests that our structural models could be useful for subsequent studies aimed at unraveling the structure of PrP^{Sc}, which is considered as a key step toward the understanding of prion diseases.[7]

ASSOCIATED CONTENT

Supporting Information

Structures of our β-rich folds in PDB format. This material is available free of charge via the Internet at http://pubs.acs.org.

AUTHOR INFORMATION

Corresponding Author

*E-mail: ursula.roethlisberger@epfl.ch. Phone: +41-(0)21-693-0321. Fax: +41-(0)21-693-0320.

Funding

Swiss National Science Foundation Grant 200020-130082 is acknowledged for funding.

Notes

The authors declare no competing financial interest.

ACKNOWLEDGMENTS

We thank the DIT/EPFL, the CSCS, and the CADMOS project for computer time.

ABBREVIATIONS

PrP, prion protein; PrP^{C}, cellular form of PrP; PrP^{Sc}, scrapie form of PrP; PrP*, metastable intermediate form of PrP; REMD, replica exchange molecular dynamics.

REFERENCES

(1) Prusiner, S. B. (1998) Prions. *Proc. Natl. Acad. Sci. U.S.A. 95*, 13363−13383.

(2) Soto, C. (2012) Transmissible proteins: Expanding the prion heresy. *Cell 149*, 968−977.

(3) Prusiner, S. (1982) Novel proteinaceous infectious particle causes scrapie. *Science 216*, 136−144.

(4) Kuwata, K., Li, H., Yamada, H., Legname, G., Prusiner, S. B., Akasaka, K., and James, T. L. (2002) Locally disordered conformer of the hamster prion protein: A crucial intermediate to PrP^{Sc}? *Biochemistry 41*, 12277−12283.

(5) Pan, K. M., Baldwin, M., Nguyen, J., Gasset, M., Serban, A., Groth, D., Mehlhorn, I., Huang, Z., Fletterick, R. J., and Cohen, F. E. (1993) Conversion of α-helices into β-sheets features in the formation of the scrapie prion proteins. *Proc. Natl. Acad. Sci. U.S.A. 90*, 10962−10966.

(6) Riek, R., Hornemann, S., Wider, G., Billeter, M., Glockshuber, R., and Wüthrich, K. (1996) NMR structure of the mouse prion protein domain PrP(121−321). *Nature 382*, 180−182.

(7) Diaz-Espinoza, R., and Soto, C. (2012) High-resolution structure of infectious prion protein: The final frontier. *Nat. Struct. Mol. Biol. 19*, 370−377.

(8) Caughey, B. W., Dong, A., Bhat, K. S., Ernst, D., Hayes, S. F., and Caughey, W. S. (1991) Secondary structure analysis of the scrapie-associated protein PrP 27−30 in water by infrared spectroscopy. *Biochemistry 30*, 7672−7680.

(9) Gasset, M., Baldwin, M. A., Fletterick, R. J., and Prusiner, S. B. (1993) Perturbation of the secondary structure of the scrapie prion protein under conditions that alter infectivity. *Proc. Natl. Acad. Sci. U.S.A. 90*, 1−5.

(10) Redecke, L., von Bergen, M., Clos, J., Konarev, P. V., Svergun, D. I., Fittschen, U. E. A., Broekaert, J. A. C., Bruns, O., Georgieva, D., Mandelkow, E., Genov, N., and Betzel, C. (2007) Structural characterization of β-sheeted oligomers formed on the pathway of oxidative prion protein aggregation in vitro. *J. Struct. Biol. 157*, 308−320.

(11) Baskakov, I. V., Legname, G., Baldwin, M. A., Prusiner, S. B., and Cohen, F. E. (2002) Pathway complexity of prion protein assembly into amyloid. *J. Biol. Chem. 277*, 21140−21148.

(12) Baskakov, I. V., Legname, G., Gryczynski, Z., and Prusiner, S. B. (2004) The peculiar nature of unfolding of the human prion protein. *Protein Sci. 13*, 586−595.

(13) Tahiri-Alaoui, A., and James, W. (2005) Rapid formation of amyloid from α-monomeric recombinant human PrP in vitro. *Protein Sci. 14*, 942−947.

(14) Post, K., Pitschke, M., Schäfer, O., Wille, H., Appel, T. R., Kirsch, D., Mehlhorn, I., Serban, H., Prusiner, S. B., and Riesner, D. (1998) Rapid acquisition of β-sheet structure in the prion protein prior to multimer formation. *Biol. Chem. 379*, 1307−1317.

(15) Jansen, K., Schäfer, O., Birkmann, E., Post, K., Serban, H., Prusiner, S. B., and Riesner, D. (2001) Structural intermediates in the putative pathway from the cellular prion protein to the pathogenic form. *Biol. Chem. 382*, 683−691.

(16) Eghiaian, F., Daubenfeld, T., Quenet, Y., van Audenhaege, M., Bouin, A.-P., van der Rest, G., Grosclaude, J., and Rezaei, H. (2007) Diversity in prion protein oligomerization pathways results from domain expansion as revealed by hydrogen/deuterium exchange and disulfide linkage. *Proc. Natl. Acad. Sci. U.S.A. 104*, 7414−7419.

(17) Baskakov, I. V., Legname, G., Prusiner, S. B., and Cohen, F. E. (2001) Folding of prion protein to its native α-helical conformation is under kinetic control. *J. Biol. Chem. 276*, 19687−19690.

(18) Leffers, K.-W., Schell, J., Jansen, K., Lucassen, R., Kaimann, T., Nagel-Steger, L., Tatzelt, J., and Riesner, D. (2004) The structural transition of the prion protein into its pathogenic conformation is induced by unmasking hydrophobic sites. *J. Mol. Biol. 344*, 839−853.

(19) Gerber, R., Tahiri-Alaoui, A., Hore, P. J., and James, W. (2008) Conformational pH dependence of intermediate states during oligomerization of the human prion protein. *Protein Sci. 17*, 537−544.

(20) Bocharova, O. V., Breydo, L., Parfenov, A. S., Salnikov, V. V., and Baskakov, I. V. (2005) In vitro conversion of full-length mammalian prion protein produces amyloid form with physical properties of PrP^{Sc}. *J. Mol. Biol. 346*, 645−659.

(21) Leffers, K.-W., Wille, H., Stöhr, J., Junger, E., Prusiner, S. B., and Riesner, D. (2005) Assembly of natural and recombinant prion protein into fibrils. *Biol. Chem. 386*, 569−580.

(22) Yu, H., Liu, X., Neupane, K., Gupta, A. N., Brigley, A. M., Solanki, A., Sosova, I., and Woodside, M. T. (2012) Direct observation of multiple misfolding pathways in a single prion protein molecule. *Proc. Natl. Acad. Sci. U.S.A. 109*, 5283−5288.

(23) Hosszu, L. L. P., Tattum, M. H., Jones, S., Trevitt, C. R., Wells, M. A., Waltho, J. P., Collinge, J., Jackson, G. S., and Clarke, A. R. (2010) The H187R mutation of the human prion protein induces conversion of recombinant prion protein to the PrPSc-like form. *Biochemistry 49*, 8729−8738.

(24) Adrover, M., Pauwels, K., Prigent, S., de Chiara, C., Xu, Z., Chapuis, C., Pastore, A., and Rezaei, H. (2010) Prion fibrillization is mediated by a native structural element that comprises helices H2 and H3. *J. Biol. Chem. 285*, 21004−21012.

(25) Hosszu, L. L. P., Trevitt, C. R., Jones, S., Batchelor, M., Scott, D. J., Jackson, G. S., Collinge, J., Waltho, J. P., and Clarke, A. R. (2009) Conformational properties of b-PrP. *J. Biol. Chem. 284*, 21981−21990.

(26) Silveira, J. R., Raymond, G. J., Hughson, A. G., Race, R. E., Sim, V. L., Hayes, S. F., and Caughey, B. (2005) The most infectious prion protein particles. *Nature 437*, 257−261.

(27) Stoehr, J., Weinmann, N., Wille, H., Kaimann, T., Nagel-Steger, L., Birkmann, E., Panza, G., Prusiner, S. B., Eigen, M., and Riesner, D. (2008) Mechanisms of prion protein assembly into amyloid. *Proc. Natl. Acad. Sci. U.S.A. 105*, 2409−2414.

(28) Rezaei, H., Eghiaian, F., Perez, J., Doublet, B., Choiset, Y., Haertle, T., and Grosclaude, J. (2005) Sequential generation of two structurally distinct ovine prion protein soluble oligomers displaying different biochemical reactivities. *J. Mol. Biol. 347*, 665−679.

(29) Lu, B.-Y., and Chang, J.-Y. (2002) Isolation and characterization of a polymerized prion protein. *Biochem. J. 364*, 81−87.

(30) Flechsig, E., Shmerling, D., Hegyi, I., Raeber, A. J., Fischer, M., Cozzio, A., von Mering, C., Aguzzi, A., and Weissmann, C. (2000) Prion protein devoid of the octapeptide repeat region restores susceptibility to scrapie in PrP knockout mice. *Neuron 27*, 399−408.

(31) Martins, S. M., Frosoni, D. J., Martinez, A. M. B., Felice, F. G. D., and Ferreira, S. T. (2006) Formation of soluble oligomers and amyloid fibrils with physical properties of the scrapie isoform of the prion protein from the C-terminal domain of recombinant murine prion protein mPrP-(121−231). *J. Biol. Chem. 281*, 26121−26128.

(32) Hornemann, S., and Glockshuber, R. (1998) A scrapie-like unfolding intermediate of the prion protein domain PrP(121−231) induced by acidic pH. *Proc. Natl. Acad. Sci. U.S.A. 95*, 6010−6014.

(33) Bocharova, O. V., Breydo, L., Salnikov, V. V., Gill, A. C., and Baskakov, I. V. (2005) Synthetic prions generated in vitro are similar to a newly identified subpopulation of PrPSc from sporadic Creutzfeldt-Jakob disease. *Protein Sci. 14*, 1222−1232.
(34) Zou, W.-Q., Capellari, S., Parchi, P., Sy, M.-S., Gambetti, P., and Chen, S. G. (2003) Identification of novel proteinase K-resistant C-terminal fragments of PrP in Creutzfeldt-Jakob disease. *J. Biol. Chem. 278*, 40429−40436.
(35) Lu, X., Wintrode, P. L., and Surewicz, W. K. (2007) β-Sheet core of human prion protein amyloid fibrils as determined by hydrogen/deuterium exchange. *Proc. Natl. Acad. Sci. U.S.A. 104*, 1510−1515.
(36) Cobb, N. J., Sönnichsen, F. D., McHaourab, H., and Surewicz, W. K. (2007) Molecular architecture of human prion protein amyloid: A parallel, in-register β-structure. *Proc. Natl. Acad. Sci. U.S.A. 104*, 18946−18951.
(37) Sun, Y., Breydo, L., Makarava, N., Yang, Q., Bocharova, O. V., and Baskakov, I. V. (2007) Site-specific conformational studies of prion protein (PrP) amyloid fibrils revealed two cooperative folding domains within amyloid structure. *J. Biol. Chem. 282*, 9090−9097.
(38) Novitskaya, V., Makarava, N., Bellon, A., Bocharova, O. V., Bronstein, I. B., Williamson, R. A., and Baskakov, I. V. (2006) Probing the conformation of the prion protein within a single amyloid fibril using a novel immunoconformational assay. *J. Biol. Chem. 281*, 15536−15545.
(39) DeMarco, M. L., and Daggett, V. (2004) From conversion to aggregation: Protofibril formation of the prion protein. *Proc. Natl. Acad. Sci. U.S.A. 101*, 2293−2298.
(40) Govaerts, C., Wille, H., Prusiner, S., and Cohen, F. (2004) Evidence for assembly of prions with left-handed β-helices into trimers. *Proc. Natl. Acad. Sci. U.S.A. 101*, 8342−8347.
(41) Wille, H., Bian, W., McDonald, M., Kendall, A., Colby, D. W., Bloch, L., Ollesch, J., Borovinskiy, A. L., Cohen, F. E., Prusiner, S. B., and Stubbs, G. (2009) Natural and synthetic prion structure from X-ray fiber diffraction. *Proc. Natl. Acad. Sci. U.S.A. 106*, 16990−16995.
(42) Chakroun, N., Prigent, S., Dreiss, C. A., Noinville, S., Chapuis, C., Fraternali, F., and Rezaei, H. (2010) The oligomerization properties of prion protein are restricted to the H2H3 domain. *FASEB J. 24*, 3222−3231.
(43) Xu, Z., Prigent, S., Deslys, J.-P., and Rezaei, H. (2011) Dual conformation of H2H3 domain of prion protein in mammalian cells. *J. Biol. Chem. 286*, 40060−40068.
(44) Smirnovas, V., Baron, G. S., Offerdahl, D. K., Raymond, G. J., Caughey, B., and Surewicz, W. K. (2011) Structural organization of brain-derived mammalian prions examined by hydrogen-deuterium exchange. *Nat. Struct. Mol. Biol. 18*, 504−506.
(45) Colacino, S., Tiana, G., Broglia, R. A., and Colombo, G. (2006) The determinants of stability in the human prion protein: Insights into folding and misfolding from the analysis of the change in the stabilization energy distribution in different conditions. *Proteins 62*, 698−707.
(46) Shamsir, M. S., and Dalby, A. R. (2005) One gene, two diseases and three conformations: Molecular dynamics simulations of mutants of human prion protein at room temperature and elevated temperatures. *Proteins 59*, 275−290.
(47) Simone, A. D., Zagari, A., and Derreumaux, P. (2007) Structural and hydration properties of the partially unfolded states of the prion protein. *Biophys. J. 93*, 1284−1292.
(48) Sugita, Y., and Okamoto, Y. (1999) Replica-exchange Molecular Dynamics Method for Protein Folding. *Chem. Phys. Lett. 314*, 141−151.
(49) Swietnicki, W., Petersen, R., Gambetti, P., and Surewicz, W. K. (1997) pH-dependent stability and conformation of the recombinant human prion protein PrP(90−231). *J. Biol. Chem. 272*, 27517−27520.
(50) Langella, E., Improta, R., Crescenzi, O., and Barone, V. (2006) Assessing the acid-base and conformational properties of histidine residues in human prion protein (125−228) by means of pK_a calculations and molecular dynamics simulations. *Proteins: Struct., Funct., Bioinf. 64*, 167−177.
(51) Campos, S. R. R., Machuqueiro, M., and Baptista, A. M. (2010) Constant-pH molecular dynamics simulations reveal a β-rich form of the human prion protein. *J. Phys. Chem. B 114*, 12692−12700.
(52) van der Kamp, M. W., and Daggett, V. (2010) Influence of pH on the human prion protein: Insights into the early steps of misfolding. *Biophys. J. 99*, 2289−2298.
(53) Antosiewicz, J., McCammon, J. A., and Gilson, M. K. (1994) Prediction of pH-dependent properties of proteins. *J. Mol. Biol. 238*, 415−436.
(54) Davis, M., and McCammon, J. (1990) Electrostatics in biomolecular structure and dynamics. *Chem. Rev. 90*, 509−521.
(55) Yang, A., Gunner, M., Sampogna, R., Sharp, R., and Honig, B. (1993) On the calculation of pK_a in proteins. *Proteins 15*, 252−256.
(56) Vriend, G. (1990) WHAT IF: A molecular modeling and drug design program. *J. Mol. Graphics 8*, 52−56 , 29.
(57) Spoel, D. V. D., Lindahl, E., Hess, B., Groenhof, G., Mark, A. E., and Berendsen, H. J. C. (2005) GROMACS: Fast, flexible, and free. *J. Comput. Chem. 26*, 1701−1718.
(58) van Gunstern, W., Billeter, S., Eising, A., Huenenberger, P., Krueger, P., Mark, A., Scott, W., and Tironi, I. (1996) *Biomolecular Simulation: The GROMOS96 Manual and User Guide*, Hochschulverlag AG, Zurich.
(59) Berendsen, H., Postma, J., van Gunsteren, W., and Hermans, J. (1981) In *Intermolecular Forces* (Pullman, B. E., Ed.) Reidel, Dordrecht, The Netherlands.
(60) Ryckaert, J. P., Ciccotti, G., and Berendsen, H. (1977) Numerical integration of cartesian equations of motion of a system with constraints: Molecular dynamics of N-alkanes. *J. Comput. Phys. 23*, 327−341.
(61) Tironi, I. G., Sperb, R., Smith, P. E., and van Gunsteren, W. F. (1995) A generalized reaction field method for molecular dynamics simulations. *J. Chem. Phys. 102*, 5451−5459.
(62) Berendsen, H., Postma, J., van Gunsteren, W., Dinola, A., and Haak, J. (1984) Molecular dynamics with coupling to an external bath. *J. Chem. Phys. 81*, 3684−3690.
(63) Nosé, S. (1984) A unified formulation of the constant temperature molecular dynamics methods. *J. Chem. Phys. 81*, 511−519.
(64) Hoover, W. (1985) Canonical dynamics-equilibrium phase space distribution. *Phys. Rev. A 31*, 1695−1697.
(65) Okur, A., Wickstrom, L., Layten, M., Geney, R., Song, K., Hornak, V., and Simmerling, C. (2006) Improved Efficiency of Replica Exchange Simulations through Use of a Hybrid Explicit/Implicit Solvation Model. *J. Chem. Theory Comput. 2*, 420−433.
(66) Yuguang, M., and Ye, Y. (2005) NIC series 34, pp 119−124.
(67) Lee, M. S., and Olson, M. A. (2010) Protein Folding Simulations Combining Self-Guided Langevin Dynamics and Temperature-Based Replica Exchange. *J. Chem. Theory Comput. 6*, 2477−2487.
(68) Cheng, X., Cui, G., Hornak, V., and Simmerling, C. (2005) Modified replica exchange simulation methods for local structure refinement. *J. Phys. Chem. B 109*, 8220−8230.
(69) Wang, J., Zhu, W., Li, G., and Hansmann, U. H. E. (2011) Velocity-scaling optimized replica exchange molecular dynamics of proteins in a hybrid explicit/implicit solvent. *J. Chem. Phys. 135*, 084115.
(70) Kabsch, W., and Sander, C. (1983) Dictionary of protein secondary structure: Pattern recognition of hydrogen-bonded and geometrical features. *Biopolymers 22*, 2577−2637.
(71) Seber, G. A. F. (1984) *Multivariate Observations*, Wiley, New York.
(72) *MATLAB* (2007) The MathWorks, Natick, MA.
(73) Kuwata, K., Kamatari, Y. O., Akasaka, K., and James, T. L. (2004) Slow conformational dynamics in the hamster prion protein. *Biochemistry 43*, 4439−4446.
(74) Ziegler, J., Sticht, H., Marx, U. C., Müller, W., Rösch, P., and Schwarzinger, S. (2003) CD and NMR studies of prion protein (PrP) helix 1. Novel implications for its role in the PrPC → PrPSc conversion process. *J. Biol. Chem. 278*, 50175−50181.

(75) Dima, R. I., and Thirumalai, D. (2004) Probing the instabilities in the dynamics of helical fragments from mouse PrPC. *Proc. Natl. Acad. Sci. U.S.A. 101*, 15335−15340.
(76) Nguyen, P. H., Li, M. S., and Derreumaux, P. (2011) Effects of all-atom force fields on amyloid oligomerization: Replica exchange molecular dynamics simulations of the Aβ(16−22) dimer and trimer. *Phys. Chem. Chem. Phys. 13*, 9778−88.
(77) Alonso, D. O., DeArmond, S. J., Cohen, F. E., and Daggett, V. (2001) Mapping the early steps in the pH-induced conformational conversion of the prion protein. *Proc. Natl. Acad. Sci. U.S.A. 98*, 2985−2989.
(78) DeMarco, M. L., and Daggett, V. (2007) Molecular mechanism for low pH triggered misfolding of the human prion protein. *Biochemistry 46*, 3045−3054.
(79) Richardson, J. S., and Richardson, D. C. (2002) Natural β-sheet proteins use negative design to avoid edge-to-edge aggregation. *Proc. Natl. Acad. Sci. U.S.A. 99*, 2754−2759.